Supporting Information

Shell Thickness Controlled Core-Shell Fe_3O_4@CoO Nanocrystals as Efficient Bifunctional Catalysts for Oxygen Reduction and Evolution Reactions

Lingshan Zhou,[a] Binglu Deng,[a] Zhongqing Jiang[b] and Zhong-Jie Jiang *[a]

[a] Guangdong Engineering and Technology Research Center for Surface Chemistry of Energy Materials &Guangzhou Key Laboratory for Surface Chemistry of Energy Materials, New Energy Research Institute, College of Environment and Energy, South China University of Technology, Guangzhou 510006, Guangdong, P. R. China. *E-mail: Zhongjiejiang1978@hotmail.com or* eszjiang@scut.edu.cn.

[b] Key Laboratory of Optical Field Manipulation of Zhejiang Province, Department of Physics, Zhejiang Sci-Tech University, Hangzhou 310018, P. R. China.

Table of Contents:

1. Experimental procedures

1.1 Chemicals

Iron acetylacetonate ($Fe(acac)_3$, 98%), cobalt acetylacetonate ($Co(acac)_2$, 97%), oleylamine (OAm, 98~99%), Tetrabutylammonium bromide (TBAB, 99%), and oleic acid (OA, 99%) were obtained from Shanghai Macklin Biochemical Technology Co. Ltd. Tri(hydroxymethyl) aminomethane (THAM, 99%) was obtained from Tianjin Damao Reagent Factory. Dopamine hydrochloride was purchased from Shanghai Aladdin Biochemical Technology Co., Ltd. Vulcan XC-72 Carbon was purchased from Shanghai Cabot Chemical Co., Ltd. Nafion (5.0 wt.%) was purchased from DuPont. All the chemicals were used directly without further purification.

1.2 Material synthesis

Synthesis of Fe_3O_4 NPs. A mixed solution of 15 mL OAm and 0.5 mL OA in a three-neck flask was heated to 160°C under the N_2 flow. 3 mL of a red $Fe(acac)_3$ solution in OAm was then injected under vigorous stirring. The reaction was last for 2 h. The obtained Fe_3O_4 NPs was centrifuge and thoroughly washed with ethanol and hexane and finally re-dispersed in hexane.

Synthesis of core@shell Fe_3O_4@CoO NCs. For the synthesis of core@shell Fe_3O_4@CoO NPs, ~0.028 g of the Fe_3O_4 NPs in 2mL hexane synthesized above was mixed with 7.5 mL OAm and 0.16 mL OA. After the removal of hexane by vacuum evaporation, the reaction system was aerated by the N_2 flow. 1.0 mL of 0.2 mmol $Co(acac)_2$ in OAm was then injected dropwise under the stirring, followed by the addition of 130 mg TBAB. The reaction solution was then heated at 110°C for 10 min. The obtained core@shell Fe_3O_4@CoO NPs were collected by centrifugation and washing with ethanol and hexane and re-dispersed in hexane. For the synthesis of the Fe_3O_4@CoO NCs with thinner and thicker shells, the reaction solution was then heated at 110°C for 5 and 30 min, respectively, while keeping other parameters constant.

1.3 Characterizations

TEM images were taken on a JEM-2100F transmission electron microscope with an accelerating voltage of 200 kV. X-ray diffraction (XRD) patterns of the catalysts were performed on a Bruker D8 Advance powder X-ray diffractometer analyzed by Bruker EVA and Bruker Top with the Cu Kα (λ=0.15406 nm) radiation. X-ray photoelectron spectroscopic (XPS) measurements were collected using a PHI X-tool instrument.

1.4 Electrochemical measurements

The NPs synthesized above were loaded on the surface of Cabot Vulcan XC-72 carbon and then coated with polydopamine (PDA) for the investigation of their electrocatalytic properties. Specifically, 20 mg of Cabot Vulcan XC-72 carbon was first dispersed in 5 mL hexane. 0.01g of Fe_3O_4@CoO NPs in 2 mL hexane was then injected. After 30 min of ultrasonication, carbon supported Fe_3O_4@CoO NPs (Fe_3O_4@CoO/C) were collected by centrifugation and re-dispersed in an aqueous solution of dopamine hydrochloride (3 mg mL^{-1}) at pH=8.5, which led to the coating of the NPs on the surface of carbon with a thin layer of PDA. The obtained product was then collected by centrifugation and dried at 60ºC, and finally transferred to a ceramic boat for calcination at 350ºC under the N_2 flow for 2 h in a tube furnace.

The preparation of the working electrode was performed using the following procedure: 3.0 mg of the as-prepared catalysts was dispersed in 1 mL solution of isopropanol, DI water and 5 wt.% Nafion (Volume ratio: 8:2:0.02) with the assistance of ultrasonication until the formation of a homogeneous ink solution. The working electrode was prepared by dropping 20 μL (0.31 mg cm^{-2}) of the ink solution on the glass carbon electrode and dried at ambient temperature. The work electrodes of 20 wt.% Pt/C and 20 wt.% RuO_2/C with loadings of ~0.30 mg cm^{-2} were prepared in a similar manner.

The catalytic performance of the samples for the ORR and OER was carried out on a computer-controlled potentiostat (CHI 760E, China) using a three-electrode system with a Pt wire as counter electrode and a KCl saturated Ag/AgCl electrode as the reference electrode, respectively. Cyclic voltammograms of the catalysts (CVs) were recorded by rotating disk electrodes (RDE) in the electrolyte solution saturated with O_2/N_2 via bubbling for >30 min. Linear scan voltammetry (LSV) was performed using a rotating disk electrode (RDE) in O_2-saturated electrolyte at a scan rate 5 mV s^{-1} with different rotation rates. The electron transfer number (n) was calculated according to the Koutecky-Levich equations:

$$\frac{1}{J}=\frac{1}{J_L}+\frac{1}{J_K}=\frac{1}{B\omega^{1/2}}+\frac{1}{J_K} \quad (1)$$

$$B=0.62\mathrm{n}FC_0D_0^{2/3}\upsilon^{-1/6} \quad (2)$$

Where J is the measured current density (mA cm^{-2}), J_L is the diffusion-limiting current density (mA cm^{-2}), J_k is the kinetic current density (mA cm^{-2}), ω the rotation rate of RDE, F is faraday constant (96485 C mol^{-1}), C_O the concentration of oxygen (1.2×10^{-3} mol L^{-1}), D_O the oxygen diffusion coefficient in 0.1 M KOH solution (1.9×10^{-5} cm^2 s^{-1}), υ the kinetic viscosity (0.01 cm^2 s^{-1}).

Rotating ring-disk electrode (RRDE) measurements were performed in the O_2-saturated 0.1 M KOH electrolytes with a scan rate of 10 mV s^{-1} at a rotation rate of 1600 rpm. The current density associated with the %HO_2^- intermediate formation was detected by the Pt ring electrode at 0.4 V vs. Ag/AgCl, which was then used to estimate the transfer electron number (n) and the percentage of the HO_2^- intermediate (%HO_2^-) using the Eqns (3) and (4).

$$n=4\times\frac{|I_D|}{|I_D|+I_R/N} \quad (3)$$

$$\%HO_2^-=200\times\frac{I_R/N}{|I_D|+I_R/N} \quad (4)$$

Where I_D is the disk current, I_R the ring current, N the current collection efficiency of the Pt ring (N=0.38).

All the OER tests were performed in the conditions similar with those of ORR at the 1600 rpm. For all the measurements, the current densities were iR-corrected with the solution resistance measured by electrochemical impedance spectroscopy (EIS) at different potentials within the frequency range of 10 kHz to 100 mHz. The potentials reported in this work were converted with respect to reversible hydrogen electrode (RHE) by the calibration equation: $E_{RHE}=E_{Ag/AgCl}+0.9653$ V (in 0.1M KOH solution). The Tafel slopes for the OER were obtained from the Tafel plots through Equation (5), which are useful to understand the rate-determining step of the OER and evaluate the catalytic activities of the catalysts.

$$\eta = a + b \cdot \log|j| \tag{5}$$

Where η denotes the overpotential, *a* the tafel constant, *b* the tafel slope and j the current density.

To demonstrate the practical applications of the samples in the Zn-air batteries, the catalysts mixed with polytetrafluoroethylene (PTFE) and coated on the nickel mesh were used as the air cathode. Zn foil as the anode. The loading of the catalyst was ~1.0 mg cm^{-2}. 0.2 M zinc acetate in a 6.0 M KOH solution was used as the electrolyte.

2. Size distribution

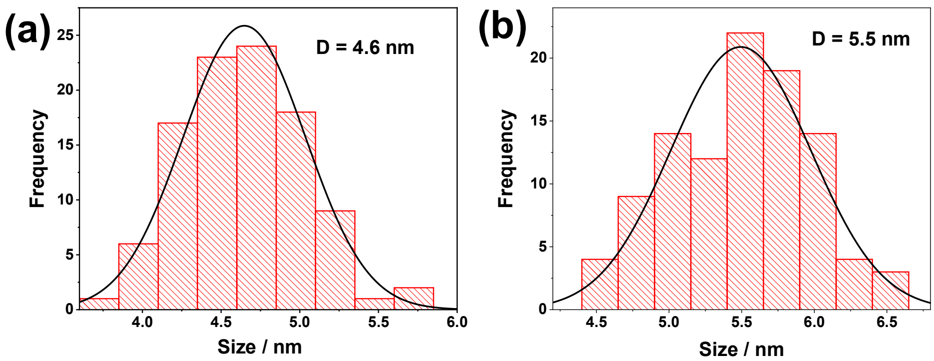

Figure S1. Size distribution histogram of (a) the Fe_3O_4 NCs and (b) the Fe_3O_4@CoO NCs.

3. XPS spectrum

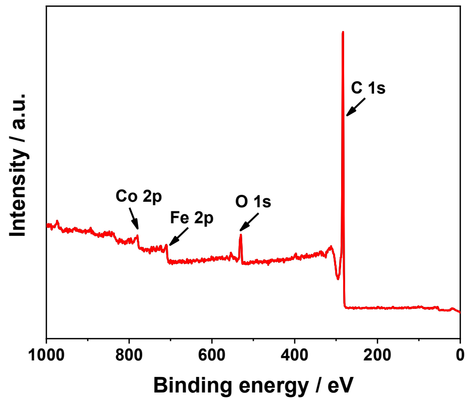

Figure S2. XPS survey spectra of the Fe_3O_4@CoO NCs.

4. Rotating ring-disk electrode (RRDE) measurements of the Fe_3O_4@CoO NCs and the Pt/C

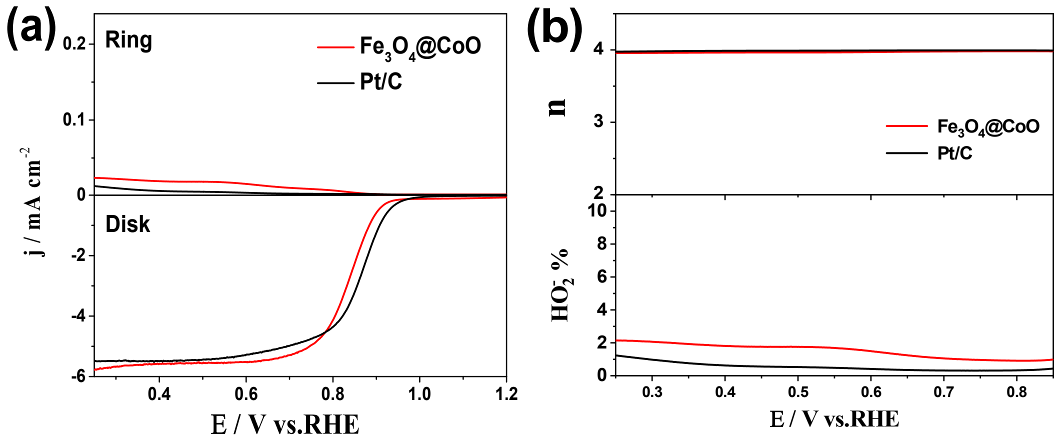

Figure S3. (a) RRDE polarization curves and (b) HO_2^- yields and electron transfer number of ORR by the Fe_3O_4@CoO NCs and the Pt/C.

5. Structure characterizations of the Fe_3O_4 NCs and the CoO NCs

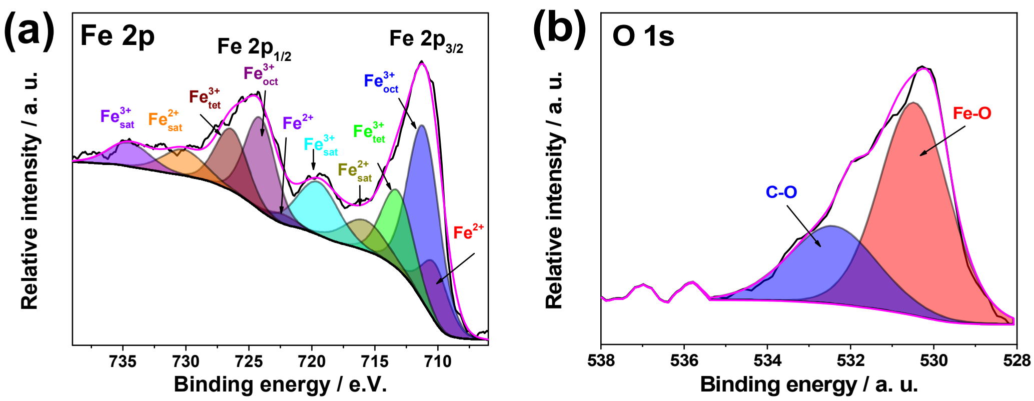

Figure S4. XPS spectra of (a) Fe 2p and (b) O 1s for Fe_3O_4 NCs.

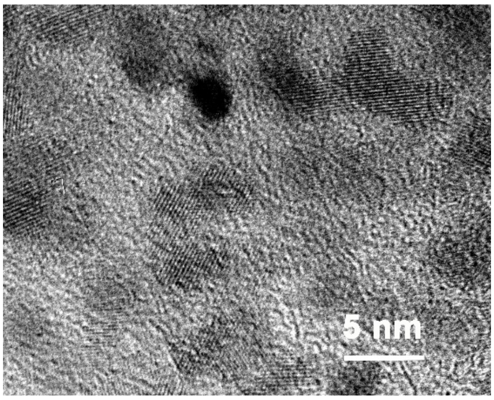

Figure S5. TEM image of CoO NCs.

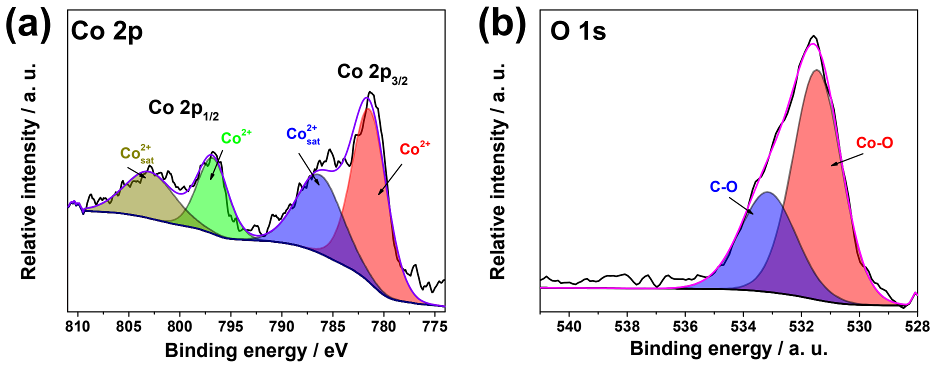

Figure S6. XPS spectra of (a) Co 2p and (b) O 1s for CoO NCs.

6. Performance comparison

Table S1. Performance comparison of the Fe_3O_4@CoO NCs with the bifunctional catalysts reported previously.

Catalyst material	Mass loading / mg cm^{-2}	E_{ORR} / V at -3 mA cm^{-2}	E_{OER} / V at 10 mA cm^{-2}	ΔE	References
Nanostructured Mn oxide	-	0.73	1.77	1.04	1
Co_3O_4/2.7Co_2MnO_4	0.2	0.68	1.77	1.09	2
$NiCo_2O_4$/graphene	0.4	0.55	1.69	1.14	3
β-MnO_2 film	-	0.76	1.78	1.02	4
α-MnO_2-SF	0.2	0.76	1.72	0.96	5
MCF/N-rGO	0.14	0.78	1.71	0.93	6
CMO/N-rGO	0.1	0.80	1.66	0.86	7
$CaMn_4Ox$	0.4	0.73	1.77	1.04	8
H-Pt/$CaMnO_3$	0.085	0.79	1.80	1.01	8
N-graphene/ CNT	0.25	0.63	1.63	1.00	9
N, P-carbon paper	-	0.67	1.63	0.96	10
Co@Co_3O_4/NC	0.21	0.74	1.64	0.90	11
$NiCo_2S_4$@N/S-rGO	0.283	0.84	1.70	0.94	12
$ZnCo_2O_4$/N-CNT	0.2	0.87	1.66	0.79	13
Co_3O_4/NHPC	0.2	0.83	1.65	0.82	14
Mn_3O_4@$CoMn_2O_4$-Co_xO_y	0.38	0.83	1.72	0.99	15
MnO_2/graphene/CNT	0.275	0.73	2.0	1.27	16
NiFeO + MnOx	0.1	0.667	1.613	0.946	17
$MnCo_2O_4$ spinel	0.1	0.659	1.646	0.98	18
$LaNiO_3$	0.1	0.700	1.58	0.88	19
$MnCo_2O_4$/N-MWCNT	0.25	0.520	1.882	1.362	20
Mn−Co oxide nanofibres	0.1	0.700	1.71	1.01	21
Mn oxide	-	0.73	1.77	1.04	22
RuO_2	0.2	0.61	1.62	1.01	1

IrO_2	0.2	0.69	1.61	0.92	1
Pt/C	0.2	0.86	2.02	1.16	1
Fe_3O_4@CoO NCs	0.31	0.829	1.623	0.79	This work

References

1. Y. Gorlin and T. F. Jaramillo, *J. Am. Chem. Soc.*, 2010, **132**, 13612-13614.
2. D. Wang, X. Chen, D. G. Evans and W. Yang, *Nanoscale*, 2013, **5**, 5312-5315.
3. D. U. Lee, B. J. Kim and Z. Chen, *J. Mater. Chem. A* 2013, **1**, 4754-4762.
4. M. Fekete, R. K. Hocking, S. L. Y. Chang, C. Italiano, A. F. Patti, F. Arena and L. Spiccia, *Energy Environ. Sci.*, 2013, **6**, 2222-2232.
5. Y. Meng, W. Song, H. Huang, Z. Ren, S. Y. Chen and S. L. Suib, *J. Am. Chem. Soc.*, 2014, **136**, 11452-11464.
6. Y. Zhan, C. Xu, M. Lu, Z. Liu and J. Y. Lee, *J. Mater. Chem. A*, 2014, **2**, 16217-16223.
7. M. Prabu, P. Ramakrishnan and S. Shanmugam, *Electrochem. Commun.*, 2014, **41**, 59-63.
8. X. Han, F. Cheng, T. Zhang, J. Yang, Y. Hu and J. Chen, *Adv. Mater.*, 2014, **26**, 2047-2051.
9. G. L. Tian, M. Q. Zhao, D. Yu, X. Y. Kong, J. Q. Huang, Q. Zhang and F. Wei, *Small*, 2014, **10**, 2251-2259.
10. T. Y. Ma, J. Ran, S. Dai, M. Jaroniec and S. Z. Qiao, *Angew. Chem. Int. Ed.* , 2015, **54**, 4646-4650.
11. A. Aijaz, J. Masa, C. Rosler, W. Xia, P. Weide, A. J. Botz, R. A. Fischer, W. Schuhmann and M. Muhler, *Angew. Chem. Int. Ed.* , 2016, **55**, 4087-4091.
12. Q. Liu, J. Jin and J. Zhang, *ACS Appl. Mater. Interfaces*, 2013, **5**, 5002-5008.
13. Z. Q. Liu, H. Cheng, N. Li, T. Y. Ma and Y. Z. Su, *Adv. Mater.*, 2016, **28**, 3777-3784.
14. J. Guan, Z. Zhang, J. Ji, M. Dou and F. Wang, *ACS Appl. Mater. Interfaces*, 2017, **9**, 30662-30669.
15. Z. Luo, E. Irtem, M. Ibanez, R. Nafria, S. Marti-Sanchez, A. Genc, M. de la Mata, Y. Liu, D. Cadavid, J. Llorca, J. Arbiol, T. Andreu, J. R. Morante and A. Cabot, *ACS Appl. Mater. Interfaces*, 2016, **8**, 17435-174444.
16. D. Ye, T. Wu, H. Cao, Y. Wang, B. Liu, S. Zhang and J. Kong, *RSC Adv.*, 2015, **5**, 26710-26715.
17. Y. Cheng, S. Dou, J. P. Veder, S. Wang, M. Saunders and S. P. Jiang, *ACS Appl. Mater. Interfaces*, 2017, **9**, 8121-8133.
18. X. Caoa, z. Chao Jina, F. Lua, Z. Yanga, M. Shenb and z. Ruizhi Yanga, *J. Electrochem. Soc.*, 2014, **161**, H296-H300.
19. W. G. Hardin, D. A. Slanac, X. Wang, S. Dai, K. P. Johnston and K. J. Stevenson, *J. Phys. Chem. Lett.*, 2013, **4**, 1254-1259.
20. X. Yu and A. Manthiram, *Catal. Sci. Technol.* , 2015, **5**, 2072-2075.

21. K. N. Jung, S. M. Hwang, M. S. Park, K. J. Kim, J. G. Kim, S. X. Dou, J. H. Kim and J. W. Lee, *Sci. Rep.*, 2015, **5**, 7665-7675.
22. X. Qiao, S. Liao, R. Zheng, Y. Deng, H. Song and L. Du, *Acs Sustain. Chen. Eng.*, 2016, **4**, 4131-4136.